Available online at www.sciencedirect.com
SCIENCE DIRECT®
European Journal of Mechanics B/Fluids 24 (2005) 296–313

Proportional control of oscillatory thermocapillary convection in a toy model

J. Shiomi, G. Amberg *

KTH Mechanics, Stockholm, S-100 44, Sweden

Received 20 March 2004; received in revised form 30 September 2004; accepted 30 September 2004

Available online 30 November 2004

Abstract

Simple model equations were formulated to examine the influence of linear feedback control on oscillations in thermocapillary convection. Limiting the solutions to have a few wavenumbers and roughly assuming the other spatial profiles, the system of equations is reduced to a set of ordinary differential equations. This toy model is able to recreate basic features of the uncontrolled system such as standing/traveling wave structures and bifurcation characteristics. The control was realized by locally heating and cooling the free surface by linearly feeding back the temperature signals measured in local positions. Implementing the proportional feedback control in this toy model, we could capture some of the essential qualitative features of the influence of the control observed in the previous experiments, including the limitation of the control. The formulation of the toy model can be used to gain physical insight in the control problem.

Keywords: Thermocapillary convection; Feedback; Control; Model; Bifurcation

1. Introduction

Oscillatory thermocapillary convection is often blamed for detrimental striations in the finished material produced by the container-less crystal growth method called floating-zone method [1]. Having the industrial motivation and advantage to be carried out in a micro-gravity condition, there have been a growing number of researches reported on the oscillatory thermocapillary convection in the past decades. Since the first experimental observation of the three-dimensional time-dependent state in thermocapillary convection by Schwabe and Scharmann [2] and Chun and Wuest [3], many works have been devoted to identify the mechanism of the instability [4–6] and to reveal the modal structures at the onset of the oscillation and their bifurcation characteristics in the supercritical regime [7,8]. Recently, flow structures for considerably high Marangoni number (*Ma*) are reported, where the flow becomes chaotic and turbulent-like [9].

With the knowledge obtained from those studies concerning the instability mechanism and bifurcation characteristics, the ultimate goal would be to suppress the oscillation. Our challenge in this report is to stabilize the flow by local modification of heat conduction on the free surface based on continuous feedback control. Some works have been reported on the control of oscillatory thermocapillary convection in various geometries.

* Corresponding author.
E-mail addresses: shiomi@mech.kth.se (J. Shiomi), gustava@mech.kth.se (G. Amberg).

0997-7546/$ – see front matter
doi:10.1016/j.euromechflu.2004.09.006

An attempt to stabilize the thermocapillary wave instability in an experiment on a plane fluid layer was made by Benz et al. [10]. The temperature signal and the phase information sensed by thermocouples near the cold end of the layer were fed forward to control a laser which heated the downstream fluid surface along a line.

A nonlinear control was performed by Petrov et al. [11,12] to stabilize the oscillation in a half-zone model by using local temperature measurements close to the free surface and modifying the temperature at different local locations. They have constructed a look-up table based on the system's response to a sequence of random perturbations. A linear control law using appropriate data sets from the look-up table was computed. The control law was updated at every time step to adapt the control law to the nonlinear system. Using one sensor/actuator pair, a successful control was observed at the sensor location for $Ma \sim 17\,750$, however infrared visualization revealed the presence of standing waves with nodes at the feedback element and the sensor. This was resolved by adding a second sensor/actuator pair, which allows the control to damp out both waves propagating clockwise and counterclockwise, thus standing waves. The performance of the control was reported for a fixed $Ma \sim 15\,000$, where the critical value was $Ma_{\mathrm{cr}} \sim 14\,000$.

This was followed by studies applying linear and weakly nonlinear control. For an annular configuration, Shiomi et al. [13,14] applied active feedback control based on a simple cancellation scheme. Active control was realized by locally modifying the surface temperature using the local temperature measured at different locations fed back through a simple control law. Using two sensor/actuator pairs, a significant attenuation of the oscillation was observed in a range of Ma, with the best performance in the weakly nonlinear regime. Applying the control on an oscillation with azimuthal wave number of 3 (mode-3), in the regime with weak nonlinearity, the oscillation was suppressed to the background noise level. The experiments also revealed the limitation of the control. When Ma is about 15% above the critical value, control fails to achieve complete suppression of the oscillation, though a significant attenuation is still achieved. The loss of control is accompanied by an increase in the amplitude of the first overtones and a modulation in the controlled signal, which may suggest the appearance of another mode triggered by the control.

Recently, with a similar method, but in a half-zone model, weakly nonlinear control of the oscillatory thermocapillary convection is reported by Shiomi et al. [15]. The experiment utilizes a unit aspect ratio liquid bridge where the most dangerous mode has an azimuthal wave number of 2 when the control is absent. The performance of control was quantified by analyzing local temperature signals and the flow structure was simultaneously identified by flow visualization. With optimal placement of sensors and heaters, proportional control can raise Ma_{cr} by more than 40%. The amplitude of the oscillation can be suppressed to less than 30% of the initial value up to 90% of Ma_{cr}. The proportional control was tested for a period doubling state to stabilize the oscillation to a periodic state. Weakly nonlinear control was applied by adding a cubic term in the control law to improve the performance of the control and to alter the bifurcation characteristics of the system.

Our earlier experimental works in proportional control have shown not only successful performance but also its limitation. In the studies in an annular geometry by Shiomi et al. [13,14], it was observed that the proportional control performs worse as the nonlinearity of the system becomes stronger. The results suggest that the limitation of control may be due to the appearance of the neighboring modes, however, this solely does not explain why the overtones are amplified. There seems to be a mechanism in the controlled system to amplify the overtones. In order to investigate the cause of the limitation and the possibility of a remedy, a toy model was formulated. Here, the intention is to construct a toy model which, at least qualitatively, reproduces important linear and nonlinear features of the system. For this purpose, limiting the number of azimuthal modes to the fundamental and first harmonic ones, and assuming the other spatial profiles, we formulate a set of ordinary differential equations. Consequently, implementing the feedback control to this toy model, we could capture some of the essential qualitative features of the influence of the control.

The model equations are addressed as *toy models* due to the extreme simplification based on rather crude assumptions. Being a *toy*, there are possibilities of discrepancies with the actual system which can certainly result in the limitation of the toy model for further application. However, such an approach is useful to reduce the complexity of the modeled system and to grow insight to the problem. Especially, when certain aspects of the system are targeted, such a toy model can be very valuable.

It should also be noted that the ultimate aim of constructing the model is to utilize it to test more sophisticated control schemes. Some of the available schemes such as the optimal control theory require the system equations to estimate the whole flow field from limited measurement information and to predict the reaction to the control. Although a more accurate model would contribute to better prediction of the system, thus better performance of control, full simulation of the Navier–Stokes equations could hardly catch up with the real time experiment in most of the flow cases. In low dimensional problems such as the current problem and the thermal convection loop presented by Bau and Torrance [16], there is a better chance that a simple set of ordinary differential equations can be sufficient, even with fairy strong nonlinearity.

The outline of the paper is as follows. Section 2 describes the formulation of the toy model. In Section 3, for the toy model with absence of control, general features of nonlinear dynamics is shown. The calibration procedure is shown in Section 4, where the model is calibrated to the annular configuration. In Section 5, control problems with feedback control are analyzed for an ideal case and a limited case with local actuation. Results are compared to the experimental results and the cause of the limitation of the control is discussed. Finally concluding remarks are addressed in Section 5.

2. The toy model

To fill the lack of understanding in how the control method influences the system, a simple model problem was formulated. By limiting the number of modes to the base tones and the first harmonics and roughly assuming the other spatial profiles, we obtained a set of ordinary differential equations by integrating the system equation following the idea of weighted residual. The model is formulated to show the basic features of the system such as standing/traveling wave structures and supercritical Hopf bifurcation.

2.1. Governing equations

The geometry of the system, as shown in Fig. 1, is a three-dimensional liquid cavity. The surface on the right side of the figure ($y = 0$) is the free surface. The intention is to model the convection in axisymetric geometries and compare the results with available experiments as well as numerical simulations, and hence periodic boundary conditions are given to the boundaries in x-direction ($x = 0, L$). The aspect ratio, A_r, defined as the ratio of the width to the height of the $y - z$ section, R/H, is set to unity throughout the current report. Thermocapillary convection is driven by imposing the temperature gradient on the free surface by heating the top wall ($z = H$) and cooling the bottom wall ($z = 0$). The temperature difference is defined as,

$$\Delta T = T(z = H) - T(z = 0) > 0. \tag{1}$$

The surface tension is considered to be a linearly decreasing function of the temperature,

$$\sigma = \sigma_0 - \gamma(T - T_0), \tag{2}$$

where γ is a positive constant. This means that the flow will be driven from top to bottom on the free surface.

The fluid is treated as a three-dimensional incompressible Newtonian liquid. Therefore, the flow is governed by the incompressible Navier–Stokes equations, energy equation and continuity equation,

$$L(\mathbf{u}) = \frac{\partial \mathbf{u}}{\partial t} + \mathbf{u} \cdot \nabla \mathbf{u} + \nabla p - \frac{Pr}{Ma} \nabla^2 \mathbf{u} = \mathbf{0}, \tag{3}$$

$$M(\theta) = \frac{\partial \theta}{\partial t} + \mathbf{u} \cdot \nabla \theta - \frac{1}{Ma} \nabla^2 \theta = 0, \tag{4}$$

$$\nabla \cdot \mathbf{u} = 0. \tag{5}$$

These equations have been nondimensionalised using the length H, temperature difference ΔT, velocity scale,

$$U = \frac{\gamma \Delta T}{\mu} \tag{6}$$

and time scale,

$$t = \frac{H}{U}, \tag{7}$$

where μ is the dynamic viscosity. The nondimensional parameters appearing above are Ma and Pr defined as,

$$Ma = \frac{\gamma \Delta T H}{\mu \alpha}, \tag{8}$$

$$Pr = \frac{\nu}{\alpha}, \tag{9}$$

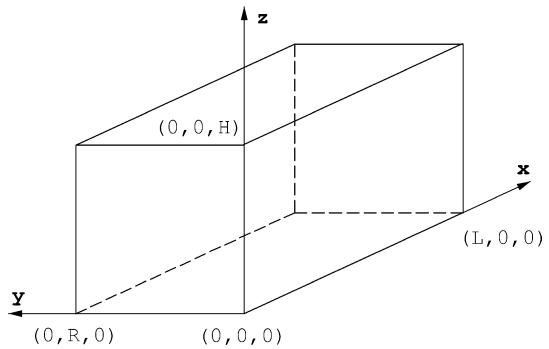

Fig. 1. Geometry.

where α and ν are the thermal diffusivity and kinematic viscosity, respectively. The equations are subjected to the boundary conditions,

$$\mathbf{u} = \mathbf{0}, \quad \theta = 0 \quad \text{at } z = 0, \tag{10}$$

$$\mathbf{u} = \mathbf{0}, \quad \theta = 1 \quad \text{at } z = 1, \tag{11}$$

$$\frac{\partial u}{\partial y} = \frac{\partial \theta}{\partial x}, \quad v = 0, \quad \frac{\partial w}{\partial y} = \frac{\partial \theta}{\partial z}, \quad \frac{\partial \theta}{\partial y} = q(x, z) \quad \text{at } y = 0, \tag{12}$$

$$\mathbf{u} = \mathbf{0}, \quad \frac{\partial \theta}{\partial y} = 0 \quad \text{at } y = A_r, \tag{13}$$

where q is the nondimensional heat flux which represents the control perturbation. The boundaries at $x = 0$ and L/H are subjected to periodic boundary conditions,

$$\mathbf{u}(x = 0) = \mathbf{u}(x = L/H), \qquad \theta(x = 0) = \theta(x = L/H). \tag{14}$$

2.2. Formulation of the toy model

In this section, the derivation of the toy model is demonstrated. The variables were separated into mean and disturbances as,

$$u(x, y, z, t) = u'(x, y, z, t), \tag{15}$$

$$v(x, y, z, t) = V(y, z) + v'(x, y, z, t), \tag{16}$$

$$w(x, y, z, t) = W(y, z) + w'(x, y, z, t), \tag{17}$$

$$\theta(x, y, z, t) = \Theta(y, z) + \theta'(x, y, z, t). \tag{18}$$

The profiles of $\Theta(y, z)$ and $W(y, z)$ are approximated as

$$W(y, z) = 4\left\{-\delta \exp\left(-\frac{y}{\delta}\right) + \delta^2 \exp(-y)\right\} z(1 - z), \tag{19}$$

$$\Theta(y, z) = z + a \exp\left(-\left(\frac{y}{\delta_T}\right)^2\right) z(1 - z). \tag{20}$$

The W profile in the y-direction was meant to have the maximum shear stress at the boundary $y = 0$. The mean temperature profile in the y-direction was chosen to have zero gradient at $y = 0$. This should be also relevant for the controlled case since we intend to control only the disturbances. a is a free parameter. δ and δ_T represent the thicknesses of the viscous and thermal boundary layers, respectively. They can be related by a straightforward scaling analysis as

$$\delta_T = \frac{\delta}{\sqrt{Pr}}. \tag{21}$$

Furthermore, based on the scaling analysis of Canright [17], we assume

$$\delta = \left(\frac{Ma}{Pr}\right)^{-1/3}. \tag{22}$$

As pointed out by Canright [17], this scaling loses accuracy as Pr becomes high, since the length scale along the free surface decreases due to the fact that more temperature change occurs in a smaller region. In the current report, this scaling was simply adopted since the z-profile of the mean temperature was modelled to have a smooth profile over the whole domain.

Substituting W to the continuity equation, we obtain

$$V(y, z) = 4\delta^2 \exp\left(-\frac{y}{\delta}\right)(2z - 1) - 4\delta^2 \exp(-y)(2z - 1). \tag{23}$$

Solving Eqs. (3)–(5) at $(y, z) = (0, 1/2)$ for mean values of the variables using Eqs. (19)–(23), we obtain

$$a = -2\frac{(\delta - 1)\delta^3 Ma}{4\delta + Pr}. \tag{24}$$

Here, for the sake of simplicity, the pressure is assumed to be,

$$p = 0. \tag{25}$$

The simplification is encouraged by the fact that the velocity profiles are modeled to satisfy continuity. Of course, more careful consideration on the treatment of the pressure term could well contribute to further modification of the toy model, but the essential physics of the convection could still be captured.

The disturbances $\mathbf{s} = \{u', w', \theta'\}$ are expanded to one pair of fundamental modes (sine and cosine) and two pairs of harmonic modes with different radial profiles as

$$\mathbf{s}(x, y, z, t) = \kappa \left\{ \mathbf{s}_{\mathbf{s},\mathbf{1}}(t) \sin(2n\pi x) + \mathbf{s}_{\mathbf{c},\mathbf{1}}(t) \cos(2n\pi x) \right\} f(y) g(z) \tag{26}$$

$$+ \kappa \left\{ \mathbf{s}_{\mathbf{s},\mathbf{2}}(t) \sin(4n\pi x) + \mathbf{s}_{\mathbf{c},\mathbf{2}}(t) \cos(4n\pi x) \right\} f(y)^2 g(z)^2$$

$$+ \kappa \left\{ \mathbf{s}_{\mathbf{s},\mathbf{2a}}(t) \sin(4n\pi x) + \mathbf{s}_{\mathbf{c},\mathbf{2a}}(t) \cos(4n\pi x) \right\} f(y)^2 g(z) \frac{\mathrm{d}g(z)}{\mathrm{d}z}, \tag{27}$$

where $\mathbf{s}_{\beta,\mathbf{k}} = \{u'_{\beta,k}, w'_{\beta,k}, \theta'_{\beta,k}\}$, $\beta = s, c$ and $k = 1, 2, 2a$. The profiles of the fluctuations are given as

$$f(y) = \exp\left(-\frac{y}{\delta'}\right), \tag{28}$$

$$g(z) = 4z(1 - z). \tag{29}$$

We assume $L = H$ without a loss of generality. The y-profiles are modeled to have maxima on the free surface for sake of simplicity. In reality, as shown by Preisser et al. [7], the peak of the fluctuation should be located in the interior. The profile $g(z)$ is designed to have a maximum at $z = 1/2$. Note that there are two pairs of harmonic modes with different z-profiles; ones with symmetric z-profile and the others with asymmetric z-profiles with respect to $z = 1/2$. Hereafter, we call the first/second pairs symmetric/asymmetric harmonic modes. This is to capture the production in the nonlinear convective terms which turns out to be essential to reproduce the oscillations.

$v'(x, y, z, t)$ can be obtained from the continuity equation as,

$$v'(x, y, z, t) = -\int_0^y \frac{\partial u'(x, \xi, z)}{\partial x} + \frac{\partial w'(x, \xi, z)}{\partial z} \, \mathrm{d}\xi. \tag{30}$$

Eqs. (3)–(5) are integrated over the entire volume, v_o, following the method of weighted residual as

$$\int_{v_o} \phi_i(x, z) L(\mathbf{u}) \, \mathrm{d}v_o = \mathbf{0} \quad (i = 1, \ldots, 6), \tag{31}$$

$$\int_{v_o} \phi_i(x, z) M(\theta) \, \mathrm{d}v_o = 0 \quad (i = 1, \ldots, 6), \tag{32}$$

where $\phi_i(x, z)$ are the test functions,

$$\begin{aligned}
&\phi_1(x, z) = \sin(2n\pi x) g(z), && \phi_2(x, z) = \cos(2n\pi x) g(z), \\
&\phi_3(x, z) = \sin(4n\pi x) g(z)^2, && \phi_4(x, z) = \cos(4n\pi x) g(z)^2, \\
&\phi_5(x, z) = \sin(4n\pi x) g(z) \frac{g(z)}{\mathrm{d}z}, && \phi_6(x, z) = \cos(4n\pi x) g(z) \frac{g(z)}{\mathrm{d}z}.
\end{aligned} \tag{33}$$

Carrying out the integrations using the boundary conditions (10)–(13) and substituting $\kappa = 1$, we obtain a set of 18 nonlinear ordinary differential equations,

$$\frac{\mathrm{d}\mathbf{x}}{\mathrm{d}t} = N'(\mathbf{x}), \tag{34}$$

for 18 variables,

$$\mathbf{x} = (\theta_{s,1}, \theta_{c,1}, \theta_{s,2}, \theta_{c,2}, \theta_{s,2a}, \theta_{c,2a}, u_{s,1}, \ldots, u_{c,2a}, w_{s,1}, \ldots, w_{c,2a})^{\mathrm{T}}. \tag{35}$$

The calibration function $D(\mathbf{x})$ is added as,

$$\frac{\mathrm{d}\mathbf{x}}{\mathrm{d}t} = N'(\mathbf{x}) + D(\mathbf{x}) = N(\mathbf{x}), \tag{36}$$

where,

$$D = (d_{s,1}, d_{c,1}, d_{s,2}, d_{c,2}, d_{s,2a}, d_{c,2a}, 0, \ldots, 0)^{\mathrm{T}}, \tag{37}$$

containing cubic terms,

$$d_{s,1} = r_1\theta'_{s,1}\theta'^2_1, \qquad d_{c,1} = r_1\theta'_{c,1}\theta'^2_1,$$
$$d_{s,2} = r_2\theta'_{s,2}\theta'^2_2, \qquad d_{c,2} = r_2\theta'_{c,2}\theta'^2_2,$$
$$d_{s,2a} = r_2\theta'_{s,2a}\theta'^2_{2a}, \qquad d_{c,2a} = r_2\theta'_{c,2a}\theta'^2_{2a},$$

where

$$\theta'_1 = (\theta'^2_{s,1} + \theta'^2_{c,1})^{0.5}, \qquad \theta'_2 = (\theta'^2_{s,2} + \theta'^2_{c,2})^{0.5}, \qquad \theta'_{2a} = (\theta'^2_{s,2a} + \theta'^2_{c,2a})^{0.5}. \tag{38}$$

r_1 and r_2 are the calibration constants which can be tuned to calibrate the toy model to match the bifurcation characteristics of the ones measured experimentally or numerically in various systems with different geometries. The details of the calibration procedure are discussed in Section 4. The thickness of the disturbance profile δ' is roughly guessed to have a physically realistic value. We set $\delta' = 0.33$ which was used throughout the current report. The mode number n was simply set to 1.

3. General features of the model system without control

In this section, the computational results of the model equations for a high Pr fluid flow without control ($q = 0$) is presented. Some of the basic features of the instability observed in earlier reported works carried out in axisymetric geometries are confirmed. Here, a typical case is shown mainly using the parameter setting $(Pr, r_1, r_2) = (14, -2.1, -50)$, however, the qualitative features shown here should be applicable to a wider range of these parameters.

3.1. Wave structure

There is an ongoing discussion about the onset wave structure of the oscillation. Many cases for different fluids and geometries are reported, which do not show agreement. In half-zone models, Savino and Monti [18] showed, performing a numerical simulation for $Pr = 30$ and $A_r = 0.5$ and 1, that the instability arises as a standing wave at the onset of the oscillation due to the symmetry of the problem but when a fully established periodic state is reached, the solution will be a traveling wave. A_r is the aspect ratio defined as the ratio of the height to radius of the liquid bridge. They mention that this is in agreement with the microgravity experiment of Monti et al. [19]. For $Pr = 4$ and 7 and A_r ranging from 0.5 to 1.3, Leypoldt et al. [8] also reported that the traveling wave is the only stable solution. On the other hand, Ueno et al. [9] performed an experiment varying the viscosity of Silicone oil $\nu = 1$–5 cSt and the aspect ratio $A_r = 0.3 - 2.0$ and found that the onset structure of the oscillation was standing.

In annular configurations, Kamotani et al. [20] observed, using a fluid with $\nu = 2$ cSt in microgravity experiments for different A_r, that the oscillation is traveling at the onset and becomes standing as Ma is increased. The same trend has been observed in a numerical simulation by [21] for $Pr = 17$. On the contrary, Lavalley et al. [22] showed in their numerical simulation that the onset oscillation is standing and becomes traveling as Ma increases. Carrying out the experiment with the same geometry as Lavalley et al. [22], Shiomi and Amberg [14] observed only traveling waves for a range of Ma with some uncertainty in judgment of the structure close to the onset. We thus observe that there is no consensus in the literature on the selection of wave structures. This, however, obviously depends sensitively on such parameters as aspect ratio, volume ratio, heat conduction through the free surface, Pr and grid resolution in case of numerical simulation.

The behavior of the current model system shows agreement with Savino and Monti [18] and Leypoldt et al. [8]. The model equations exhibit only a traveling wave as a stationary solution. However, depending on the initial condition and the strength of nonlinearity, it does become standing as a quasi-stationary state. The subfigures in Fig. 2 show typical pictures of time histories of oscillation in the weakly nonlinear regime, where $\theta'_{s,1}$ and $\theta'_{c,1}$ are marked with solid and dotted lines, respectively. As seen in the left subfigure, when the initial condition is small enough, $\theta'_{s,1}$ and $\theta'_{c,1}$ are in phase, hence the oscillation is standing. Both the amplitude and the phase remains almost constant for more than 200 periods of oscillation, where the duration of one period is typically about 2 seconds. In the figures, the time is dimensionalized using the physical properties from the experiment of Shiomi et al. [13,14]. Eventually, the oscillation begins to travel and reaches the stationary traveling state as observed in the right subfigure. Here, $\theta'_{s,1}$ and $\theta'_{c,1}$ oscillate with the same amplitude and $\pi/2$ phase difference, which suggests the traveling wave.

The transition from standing to traveling wave can be best described by computing the amplitudes of two waves propagating in the opposite direction. Here, we define $A_{i,+}(t)$ and $A_{i,-}(t)$ as the amplitudes of the ith mode wave propagating in positive and negative directions along the x-axis. In Fig. 2, the time histories of the $A_{i,+}(t)$ and $A_{i,-}(t)$ decomposed from $\theta'_{s,1}$ and $\theta'_{c,1}$ (Appendix) are denoted by dotted-dashed and dashed lines, respectively. It can be observed that after the initial growth of

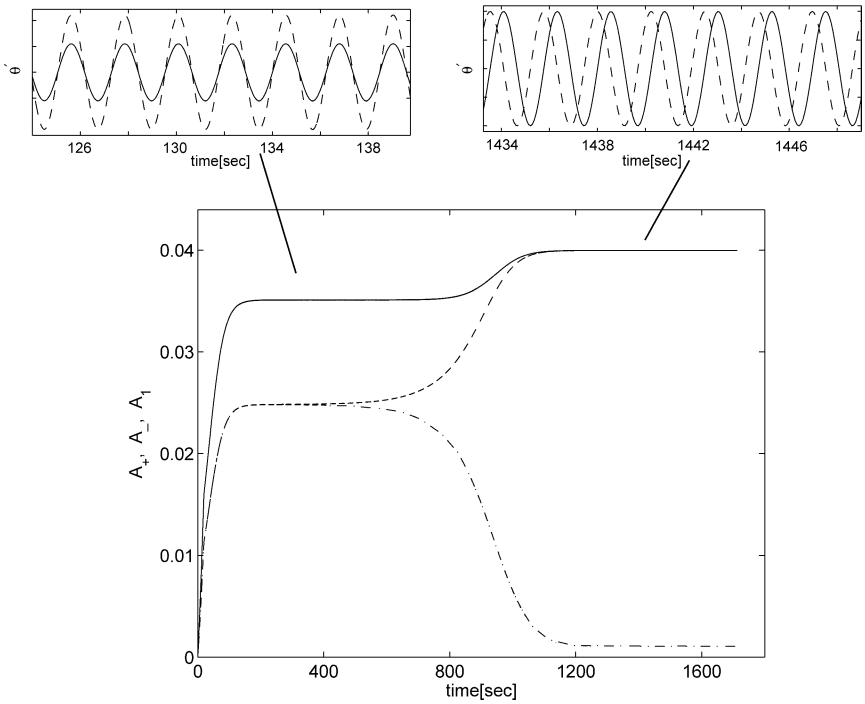

Fig. 2. Amplitude of waves of the fundamental modes with opposite direction of propagation in x-direction. (—, − −, − · −) denote $(A_1(t), A_{i,+}(t), A_{i,-}(t))$. $(Ma, Pr, r_1) = (1600, 14, -2.1)$.

oscillation, the amplitudes of the standing wave show almost no change until around $t = 700$. Then through the transient state, the oscillation gradually turns into a pure traveling wave, where the amplitudes of $\theta'_{s,1}$ and $\theta'_{c,1}$ become the same. This observation of quasi-stationary state supports the results reported by Monti et al. [19]. The total amplitude of the ith mode oscillation is defined as

$$A_i(t) = \sqrt{A_{i,+}(t)^2 + A_{i,-}(t)^2}, \tag{39}$$

which is marked by a solid line in the figure.

For the above case, the local maxima and minima of the harmonic modes are plotted in Fig. 3. Solid, dashed, dotted and dot-dashed lines denote the local maxima and minima of $\theta'_{s,2}$, $\theta'_{c,2}$, $\theta'_{s,2}$ and $\theta'_{c,2}$, respectively. Among the harmonic terms, $\theta'_{s,2}$ and $\theta'_{c,2}$ follow the trends of fundamental ones, whereas $\theta'_{s,2a}$ and $\theta'_{c,2a}$ exhibit the mean value deviating from zero. This implies that there is a mean heating due to the nonlinear interaction in the system equations.

3.2. Bifurcation characteristics

In previous numerical and experimental reports on the oscillatory thermocapillary convection in various geometries such as half-zone models [8,15] and annular configurations [22,13,14], it was observed that the flow shows a supercritical Hopf bifurcation where the amplitude of the oscillation increases linearly with the square root of ϵ in the weakly nonlinear regime. ϵ is the over-critical parameter defined as,

$$\epsilon = \frac{Ma - Ma_{\mathrm{cr}}}{Ma_{\mathrm{cr}}}. \tag{40}$$

As discussed by Leypoldt et al. [8], if the amplitudes of the two traveling waves with opposite rotation were to take a form of the general Ginzburg–Landau equations, when $A_+ \gg A_-$ or $A_+ \ll A_-$ as seen in the current study, A_1 should exhibit Hopf bifurcation in the weakly nonlinear limit. As the nonlinearity becomes stronger, the data fall off from the curve. Especially, in Leypoldt et al. [8], it is shown that these trends can be seen in all the harmonic modes containing significant energy.

These qualitative trends are well recreated by the toy model as shown in Fig. 4, where typical bifurcation curves computed by the model equations are depicted. The solid lines mark the amplitude of the fundamental and symmetric harmonic modes, A_1 and A_2. A_i is a time-dependent variable, however since in the current report it is mostly used to compute the amplitudes

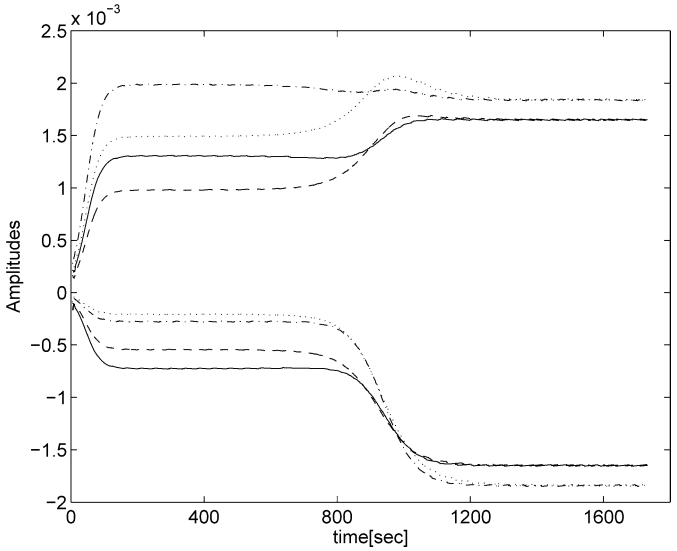

Fig. 3. Maxima and minima of the oscillation of the harmonics modes. (—, −−, ⋯, − · −) denote the local maxima and minima of $(\theta'_{s,2}, \theta'_{c,2}, \theta'_{s,2}, \theta'_{c,2})$. $(Ma, Pr, r_1) = (1600, 14, -2.1)$.

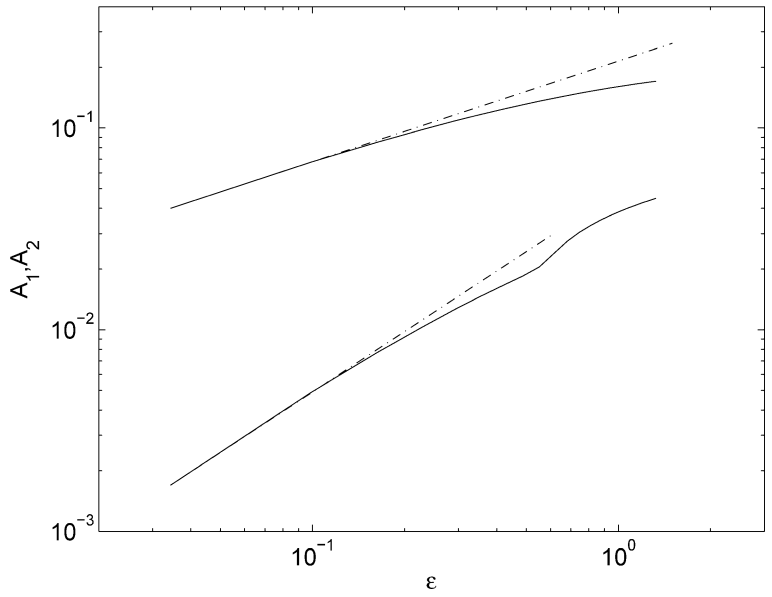

Fig. 4. Bifurcation diagram. (—), amplitudes computed by the model (top: A_1, bottom: A_2). (− · −), Hopf bifurcation curve fitted in weakly nonlinear regime. $(Pr, r_1, r_2) = (14, -2.1, -50)$.

for saturated oscillations, the time dependence is omitted unless it is specified. For the harmonic modes, the amplitudes were computed for only the symmetric modes as, in the experiment, temperature signals were measured at the midgap ($z = 1/2$) where the asymmetric modes have nodes.

Ma_{cr} was determined by extrapolating the bifurcation curve to $A_1 = 0$. For this particular case, Ma was 1547. The dotted-dashed lines represent the least square fits to the data in the weakly nonlinear regime, $\epsilon \ll 1$. When $\epsilon \ll 1$, the result is in a good agreement with the Hopf bifurcation where the squared amplitude increases linearity with ϵ. The trends in how the computed amplitudes go off from the fitted lines at $\epsilon \sim 0.2$ and how the slope of the bifurcation curve increases for higher modes agree well with the results of Leypoldt et al. [8].

When the value of ϵ exceeds a certain value ($\epsilon \sim 0.5$), the state bifurcates to a quasi-periodic oscillation. Fig. 5(a), depicts the three-dimensional return map constructed from time series of temperature signal at $x = 0$ for $\epsilon = 0.81$. The delay dt is set

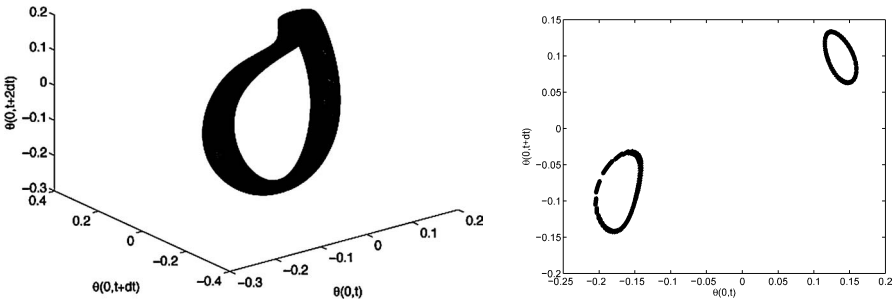

(a) (b)

Fig. 5. (a): A three-dimensional return map of $\theta'(0.t)$, $\epsilon = 0.75$, (b): A two-dimensional section ($\theta'(0, t + 2\,\mathrm{d}t) = 0$) of the return map.

to be 0.118 seconds in physical time. The map has a form of torus as can be better understood from a two-dimensional section of the three-dimensional map shown in the Fig. 5(b). The section is taken at $\theta(0, t + 2\,\mathrm{d}t) = 0$. The result is contradictory to the experimental observation of Shiomi et al. [15] in a half-zone where the scenario to chaos was shown to be through period-doubling.

In Fig. 4, when the oscillation becomes quasi-periodic, the amplitudes A_i cannot be computed as Eq. (39), hence in this regime, A_i was computed as the square root of summation of variance of $\theta'_{i,s}$ and $\theta'_{i,c}$. This was also done when computing the amplitudes of the controlled oscillation. It should be noted that the bifurcation characteristics of the fundamental and harmonic modes in the periodic regime is independent of r_2. It is only r_1 which determines the slope of the Hopf bifurcation. r_2 governs the bifurcation characteristics of the second bifurcation to the quasi-periodic state in terms of the critical value of ϵ and the volatility of the disturbance.

4. Modeling the flow in annular configurations

The model equations are provided with the third order terms in Eq. (37) to be calibrated to match the bifurcation curves of the given system. In this report, oscillatory thermocapillary convection in an annular configuration is modeled. The target system is the experiment performed by Shiomi and Amberg [14].

4.1. The annular configuration

In an annular configuration, first suggested by Kamotani et al. [23], a generic flow of a character similar to that found in the float zone method can be studied. As shown in Fig. 6, in the experiment carried out by Shiomi and Amberg [14], the system is an open cylindrical container filled with liquid to have a flat free upper surface. A heated pipe with a prescribed temperature is located on the axis of the container. The outer cylindrical wall is maintained at a lower temperature. Thermocapillary convection is thus driven by imposing a radial temperature gradient on the flat free surface. The bottom temperature condition is adiabatic. In experiments, this geometry has one advantage that, having the free surface perpendicular to gravity, it can be kept flat, thus better quantitative analysis can be achieved. The aspect ratio A_r, ratio between the height of the fluid H and the radius of the cell R, was kept at unity. The ratio of the diameter of the heated pipe R_h to R is $H_r = 0.21$. More details of the apparatus and procedure of the experiment are given in Shiomi and Amberg [14].

4.2. Calibration

To give freedoms to the model equations to follow the bifurcation characteristics of the given system, third order terms (37) were added to the model equations. As stated earlier, the value of r_1 decides the slope of the bifurcation curves and, more importantly, the ratio between the magnitude of fundamental and harmonic modes. The value of r_2 governs the stability characteristics of the second bifurcation to the quasi-periodic state namely criticality and the $\partial A_2/\partial\epsilon$ of the bifurcation. Therefore, the calibration was mainly done by determining the optimal value of r_1, which minimizes the error,

$$\int_0^{\epsilon_0} (\gamma'_e - \gamma_e)^2\,\mathrm{d}\epsilon, \tag{41}$$

where γ'_e and γ_e are the ratio of energy of the first harmonic to fundamental frequency of the toy model solution and the experiment, respectively. ϵ_0 is the maximum ϵ explored in the experiment ($\epsilon_0 = 0.42$). In Fig. 7, γ'_e and γ_e are shown for

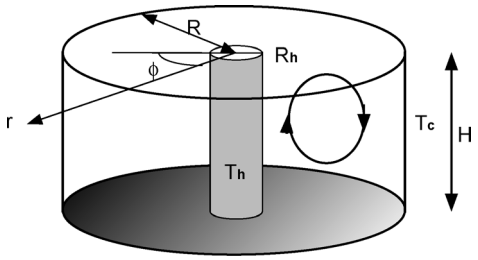

Fig. 6. Annular configuration.

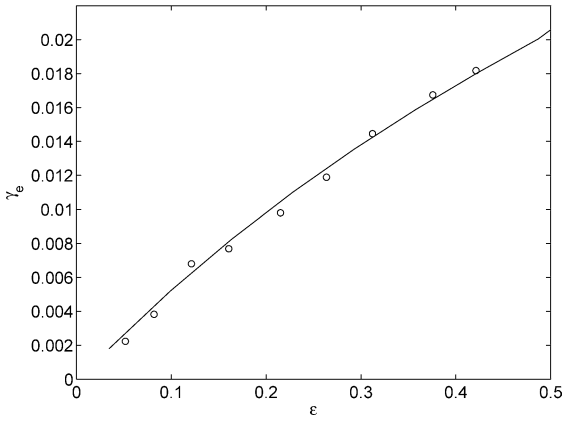

Fig. 7. Calibration of the toy model using the energy ratio of fundamental to first harmonic frequency, γ_e. Solid line: the calibrated toy model. Circles: experimental data [14].

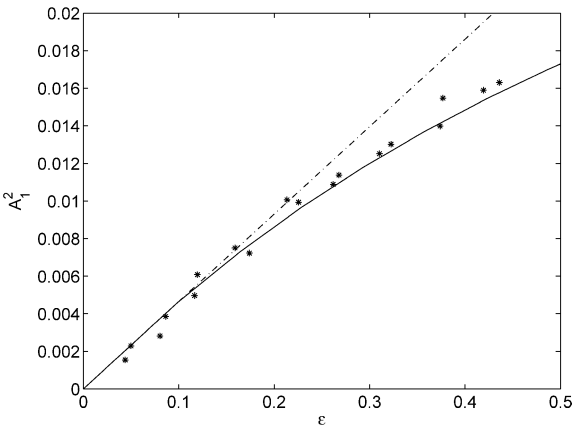

Fig. 8. Bifurcation curves. Solid line: the calibrated toy model. Stars: the scaled experimental data [14]. Dash-dotted line: $A_1^2 \propto \epsilon$.

a range of ϵ. The value of r_2 is determined so that the quasi-periodic state exhibits realistic volatility. In the present study, $r_2 = -50$ is chosen.

In order to compare the bifurcation curve of the model with that of the experiment, the experimental data are scaled as

$$\theta'_e(x,t) = \beta\theta'_m(x,t), \tag{42}$$

where θ'_m is the local free-surface temperature of the fundamental mode measured in the experiment and β is a constant. It is natural that the experimental data need to be scaled to be compared to the solution of the model problem since the experiment measures the local temperature while the solutions to the model are integrated in space. Of course, main part of the discrepancy in the quantities is due to the fact that the model is a *toy*. In fact, this scaling is not necessary if one only considers the application to control problem since it will be overshadowed by the control gain, however, it is still beneficial to compare two results in terms of the the shape of bifurcation curve as shown in Fig. 8. In the figure, A_1^2 (solid line) is plotted together with the squared amplitude of θ'_e for $\beta = 8.45$ (stars). The dotted-dashed line represents the Hopf bifurcation curve as in Fig. 4. Very good agreement with the experimental results can be observed. Note that the only parameters modified for the calibration are the constants r_1 and β, hence it is fair to say that the good agreement in the entire range of ϵ is owing to the fact that the qualitative features of the phenomenon are captured in the model system.

5. Linear feedback control of the nonlinear system

In the current report, we intend to identify the cause of the limitation of the control observed in the experiment of Shiomi and Amberg [14], which is accompanied with an increase in the amplitude of the first overtone for large ϵ (> 0.15). Following the idea of the proportional control performed in our previous experimental works, we apply a linear feedback law,

$$q(x_i + dx) = -G_1\theta'(x_i), \tag{43}$$

where x_i, represent the sensor positions and dx is the distance from the sensor to the corresponding actuator along the x-axis. G_1 is the linear control gain. In the experiments, dx is determined so that the temperature signals at the sensor and the

corresponding actuator are in phase. With this, a simple cancellation scheme can be constructed. Two sensor/actuator pairs (controllers) were used in the experiments to cover the two degrees of freedom in azimuthal rotation of the wave. Since, in the current computation, it is possible to place a sensor and a heater at the same location, we can set the value of dx to 0 without losing the correspondence to the experiments.

5.1. Linear control problem

A formulation of a linearized system enables us to treat the problem in rather classical manner of the linear control theory. On solving the equation system (31) and (32) for the first order ($\kappa^2 \ll \kappa$), a linear control problem of the system equation can be formulated as,

$$\frac{\mathrm{d}\mathbf{x}}{\mathrm{d}t} = \mathbf{A_L}\mathbf{x} + \mathbf{B}\mathbf{q}, \tag{44}$$

$$\mathbf{y} = \mathbf{C}\mathbf{x}, \tag{45}$$

where $\mathbf{A_L}$ is an 18×18 system matrix containing elements which are functions of Ma. In the linear system, the fundamental modes and harmonic modes are decoupled and so as the sine and cosine modes. The input matrix

$$\mathbf{B} = \begin{bmatrix} \mathbf{B}_\theta \\ \hline \mathbf{0} \end{bmatrix} \tag{46}$$

and input $\mathbf{q}$ are determined by the design of the actuation. $\mathbf{B}_\theta$ is a submatrix of $\mathbf{B}$ representing the input to the temperature equations. $\mathbf{y}$ is the observed measurements deduced from the state vector $\mathbf{x}$ according to the matrix $\mathbf{C}$.

5.2. Feedback control

The linear feedback control scheme can be written as

$$\mathbf{q} = \mathbf{K}\mathbf{y}, \tag{47}$$

where the linear gain $\mathbf{K}$ is a square matrix with dimension of the measurements. Here, based on the previous experiments, we consider a simple case $\mathbf{K} = G_1\mathbf{I}$, where $\mathbf{I}$ is the identity matrix. Now, the linear system with feedback loop can be written as,

$$\frac{\mathrm{d}\mathbf{x}}{\mathrm{d}t} = [\mathbf{A_L} - G_1\mathbf{B}\mathbf{I}\mathbf{C}]\mathbf{x}. \tag{48}$$

5.3. Ideal control

Before exploring the possibility to model the controlled system in the experiments, let us examine the control in more ideal situation. In this section, we try to exclude the complication caused by the fact that the temperature is measured locally and control is applied locally in the experiments. Now, we expand the non-dimensional heat flux q in the same manner as for the state variables,

$$\begin{aligned} q(x,z,t) = {} & \left\{q_{s,1}(t)\sin(2\pi x) + q_{c,1}(t)\cos(2\pi x)\right\}g(z) + \left\{q_{s,2}(t)\sin(4\pi x) + q_{c,2}(t)\cos(4\pi x)\right\}g(z)^2 \\ & + \left\{q_{s,2a}(t)\sin(4\pi x) + q_{c,2a}(t)\cos(4\pi x)\right\}g(z)\frac{\mathrm{d}g(z)}{\mathrm{d}z}. \end{aligned} \tag{49}$$

Substituting this into (12) on formulating the linear or nonlinear system gives

$$\mathbf{q} = (q_{s,1}, q_{c,1}, q_{s,2}, q_{c,2}, q_{s,2a}, q_{c,2a})^{\mathrm{T}}. \tag{50}$$

Accordingly, $\mathbf{B}$ is an 18×6 matrix. Inheriting the idea from the experiment to maintain some correspondences, the matrix $\mathbf{B}$ was designed so that we act on the equation of each mode only with the perturbation with the same mode. We define three alternatives for $\mathbf{B}$ with diagonal forms of $\mathbf{B}_\theta$; The first one simulates the case where we can modify only the fundamental temperature modes ($\mathbf{B_1}[k,k] = 0$, $k = 3,\ldots,6$). The second one is for the case where we can also modify the symmetric harmonic modes ($\mathbf{B_2}[k,k] = 0$, $k = 5, 6$). Finally, the third one for the case where all the temperature modes can be modified ($\mathbf{B_3}$).

Now, we examine the controllability of the system. When the system can be transfered from any initial condition to any desired state in a finite time by proper choice of input $\mathbf{q}$, the system is linearly controllable. The criterion is that the rank of the controllability matrix, $\Gamma = \mathrm{rank}[\mathbf{B}, \mathbf{A_L}\mathbf{B}, \ldots, \mathbf{A_L^{17}}\mathbf{B}]$, is a full rank, in other words, the matrix is nonsingular [24]. Similarly, the system is observable if, for given $\mathbf{y}$ and $\mathbf{q}$, the initial state can be deduced. The criterion for this is given by $\Omega = \mathrm{rank}[\mathbf{C}^{\mathrm{T}}, (\mathbf{A_L^T})^2\mathbf{C}^{\mathrm{T}}, \ldots, (\mathbf{A_L^T})^{17}\mathbf{C}^{\mathrm{T}}]$ to be a full rank.

Checking the criterion for controllability for $\mathbf{B_1} \sim \mathbf{B_3}$, we obtain

$$\Gamma|_{\mathbf{B}=\mathbf{B_1}} = 9, \tag{51}$$

$$\Gamma|_{\mathbf{B}=\mathbf{B_2}} = 18, \tag{52}$$

$$\Gamma|_{\mathbf{B}=\mathbf{B_3}} = 18, \tag{53}$$

independently of *Ma* ($0 < \epsilon < 0.5$). Therefore, at least, modification of both fundamental and harmonic symmetric mode pairs is necessary for the linear system to be controllable, i.e. to assure the existence of $\mathbf{q}$ with which the state can be transfered to the target state.

The analysis for the observability of the linear system would give the same result. Therefore, if we are to detect one mode with one sensor for a certain time interval, we would need at least 4 sensors to be able to estimate the initial condition for the rest of the state variables from the measured data using the linear system.

From the knowledge obtained above, the feedback control can be designed such that measurements and actuation are done for only the symmetric modes, i.e. $\mathbf{B} = \mathbf{B_2}$. Similarly, the measurements are limited to symmetric modes which corresponds to the experiment where asymmetric modes cannot be detected with sensors positioned in the midgap. This gives $\mathbf{C}[k,k] = 1$, $k = 1, \ldots, 4$, and 0 in the other elements.

For the above design of control, the stability of the linear control system (48) can be examined. Consequently, all the eigenmodes were found to be stable for large enough values of G_1. The threshold value of G_1 increases with ϵ.

On applying the feedback to the nonlinear system (36) the nonlinear saturated state without control was given as the initial condition. The resulting performance of the control is characterized by drawing the bifurcation curves for various values of G_1. In Fig. 9, the bifurcation curves for A_1, A_2, and $(A_1^2 + A_2^2)^{1/2}$ are shown. It can be observed that all the amplitudes monotonically decrease with increasing G_1. This shows that with a large enough G_1, the oscillation can be completely suppressed by the linear control.

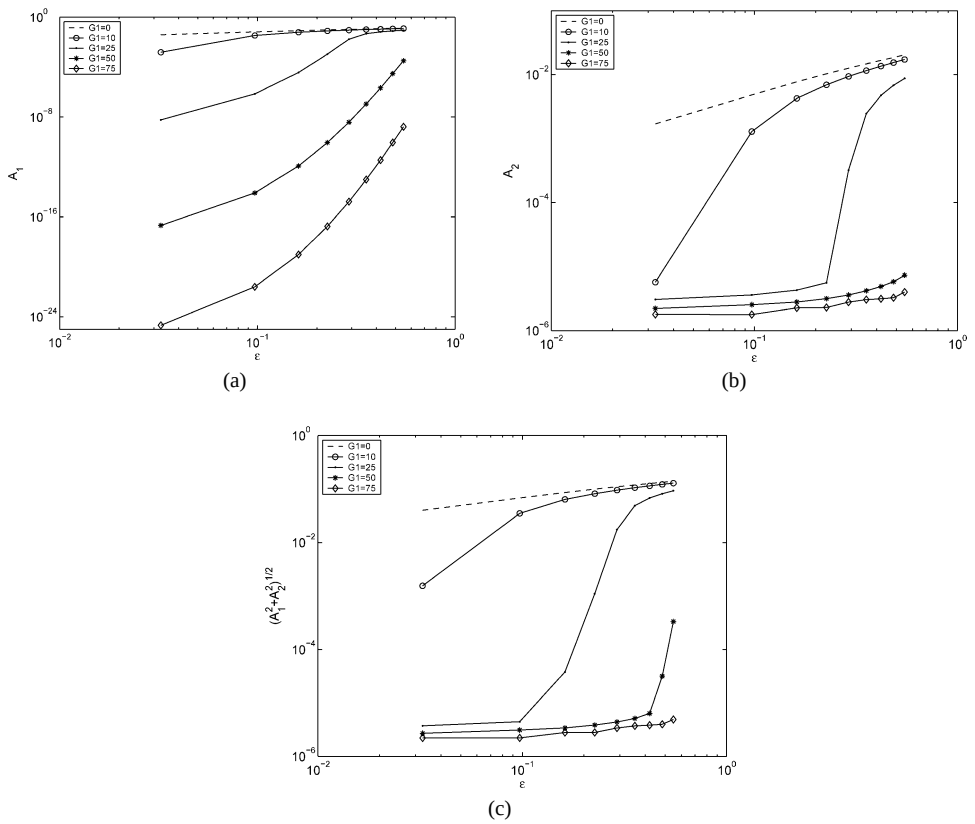

Fig. 9. Bifurcation diagrams of the toy model subjected to the *ideal* control. (a) Fundamental modes, (b) harmonic modes, (c) overall.

5.4. Feedback control with point heat sources

In the experiment, the control is done by locally measuring and modifying the temperature boundary condition on the free surface using two controllers. Compared with the previous ideal case, the spatial locality in both measurement and actuation should cause more complications. To examine the cause of the limitation of the control, the model problem is formulated with the boundary condition,

$$q(x,z,t) = q_1(t)h(z)\exp\left[-\left(\frac{\Delta x}{x-x_1}\right)^2\right] + q_2(t)h(z)\exp\left[-\left(\frac{\Delta x}{x-x_2}\right)^2\right], \tag{54}$$

where Δx represents the length of actuators in the x direction. Δx is given the value 0.025, which corresponds to the size of the actuators used in the experiment. The x-profile of the output from the actuator is estimated with a gaussian function. When carrying out the integration in Eqs. (31) and (32), we give different z-profiles, $h(z) = g(z)$, $g(z)^2$ and $g(z)\mathrm{d}g(z)/\mathrm{d}z$, for the fundamental, symmetric harmonic and asymmetric harmonic modes. This is to fit the z-profile of the actuation to the wave of each mode, in order to focus on the examination of the influence of locality in x-direction. Consequently, we obtain $\mathbf{B}$ as a function of x_1 and x_2, which is named $\mathbf{B_p}$ hereafter. The inputs are $\mathbf{q} = [q_1, q_2]^{\mathrm{T}}$.

As in the experiment, the temperature is measured at two locations $\theta'(x_1, 0, 1/2, t)$ and $\theta'(x_2, 0, 1/2, t)$. We find the matrix $\mathbf{C}$ for this case,

$$\left\{\mathbf{C_p}[i,1], \mathbf{C_p}[i,2], \mathbf{C_p}[i,3], \mathbf{C_p}[i,4]\right\} = \{\sin 2\pi x_i, \cos 2\pi x_i, \sin 4\pi x_i, \cos 4\pi x_i\}, \quad i = 1,2, \tag{55}$$

with 0 elements otherwise. Now, giving $x_1 = 0.25$ and $x_2 = 0.5$, which correspond to the optimal positioning of the controllers report by Shiomi and Amberg [14], we obtain $\mathbf{C_p}[1,1] = \mathbf{C_p}[2,4] = 1$, $\mathbf{C_p}[1,4] = \mathbf{C_p}[2,3] = -1$ and 0 in the rest of the elements.

The local feedback can be realized as Eq. (47), where, based on the experiment, $\mathbf{K}$ is designed to be $\mathbf{K} = -G_1\mathbf{I}$ with $\mathbf{I}$ as the identity matrix of second order. Our original idea, on designing $\mathbf{K}$, was to target only the fundamental mode, considering the harmonic modes to be the secondary phenomena resulting from the nonlinear dynamics of the fundamental oscillation. The non-diagonal elements of the gain matrix $\mathbf{K}$ would represent the coupling between the controllers. Since the state variables and the control do not have the same profiles with the local actuation, it is possible that finite values of non-diagonal elements can contribute to the efficiency of the opposition. This was investigated by carrying out a simple estimation considering the opposition of only the fundamental modes (Appendix). Consequently, it was found that the $\mathbf{K}$ with the best opposition can be considered as diagonal matrix for $\Delta x = 0.025$. Hence, from the symmetry of the system, $\mathbf{K}$ was designed take the form as stated above. The same analysis could be carried out for the full linear system including harmonic modes, however, then we would violate the limit on the number of sensors in the experiment.

5.4.1. Bifurcation curves

For the nonlinear system with the feedback loop, bifurcation curves for different values of G_1 are plotted in Fig. 10(a)–(c). In this case, none of the amplitudes show monotonic decrease. As shown in Fig. 10(a), increasing G_1 for certain value of ϵ, A_1 decreases until G_1 reaches a certain value, and then it increases again. However, the suppression is achieved for all the parameters, G_1 and ϵ explored in the current report.

On the other hand, as shown in Fig. 10(b), it was observed that the harmonic modes can be destabilized with excess G_1. For $\epsilon \leqslant 0.38$, the harmonic modes can be attenuated to some extent, but as G_1 exceeds certain values, A_2 begins to increase with G_1 and eventually exceeds the initial amplitude without control. For $\epsilon \geqslant 0.38$, A_2 shows monotonous increase with G_1. In this regime, control has a destabilizing effect on the harmonic modes.

The bifurcation curves shown in Fig. 10(c) reflect the influence of the control on the total energy of the oscillation. For the examined range of ϵ, the total amplitude decreases as G_1 increases from 0. At certain values of G_1 depending on the value of ϵ, the amplitude reaches the minima. We define this optimal value of G_1 as $G_{1,\mathrm{opt}}$. As G_1 exceeds $G_{1,\mathrm{opt}}$, the amplitude monotonically increases.

5.4.2. Overall performance

The overall performance of the control is demonstrated in Fig. 11(a) where the suppression ratio for $G_1 = G_{1,\mathrm{opt}}$ is plotted for a range of ϵ. The suppression ratio γ is defined as the ratio of controlled total amplitude to the uncontrolled one. It can be seen that, in the weakly nonlinear regime ($\epsilon \leqslant 0.28$), the control achieves complete suppression of the oscillation, i.e. the Ma_{cr} was raised by 28%. Beyond the threshold value, γ increases as the nonlinearity becomes stronger.

The result qualitatively agrees very well with the experiment by Shiomi and Amberg [14] whose corresponding result is shown in Fig. 11(b). Both show complete attenuation of the oscillation in the weakly nonlinear regime, then a sudden increase of G_1 after reaching the threshold values of ϵ. Note that in the experiment, measurement noise was approximately 10% of the uncontrolled signals in the weakly nonlinear regime, hence γ does not become less than 0.1.

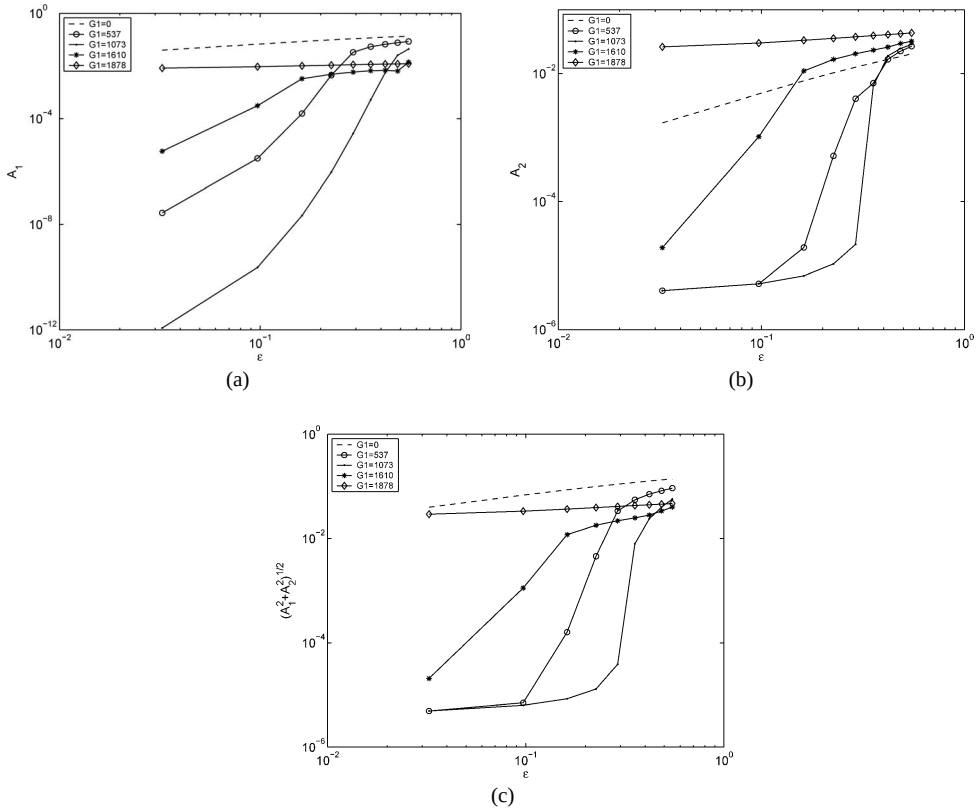

Fig. 10. Bifurcation diagram of the toy model subjected to the local control. (a) Fundamental modes, (b) harmonic modes, (c) overall.

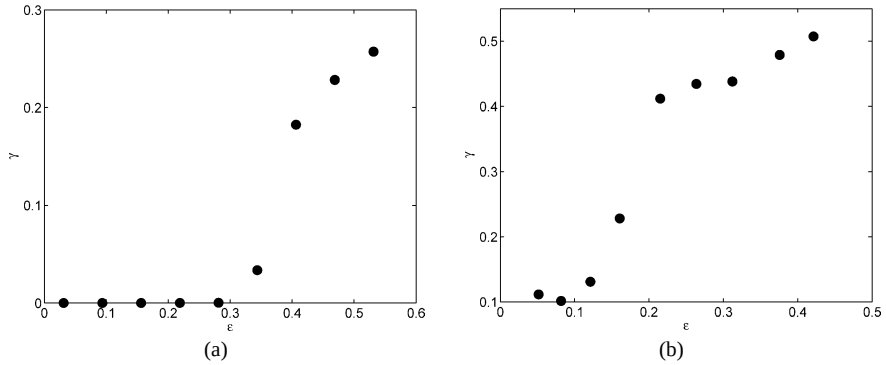

Fig. 11. The overall performance of the proportional control of (a): model equation system and (b): experiments. γ: suppression ratio, the ratio of amplitude controlled with the optimal gain to uncontrolled.

The increase of γ is accompanied with the amplification of the harmonic modes. In order to compare the current model system with the experiment in this respect, the energy ratios in harmonic modes for the toy model and the experiment are plotted in Figs. 12 (a) and (b), respectively. In Fig. 12(a), E_2 and $E0_2$ represent the energy in the harmonic modes of the controlled (with $G_{1,\mathrm{opt}}$) and uncontrolled oscillation. Similarly, in Fig. 12(b), $E0_{\mathrm{hf}}$ and E_{hf} are the energies of harmonic frequency. If we assume that, in the experiment, most of $E0_{\mathrm{hf}}$ and E_{hf} belong to the oscillation with harmonic wavenumber, good qualitative agreement could be obtained between the two results, where the energy of the harmonic mode with control rapidly increases at certain ϵ and reaches almost triple the original value without control.

It is possible to comment on the cause of the amplification of the harmonic modes by observing the power spectra of the controlled oscillation. In Fig. 13, the power spectra of fundamental and symmetric harmonic modes of controlled oscillation are plotted together with those of uncontrolled ones. The spectra for controlled/uncontrolled oscillations are depicted by

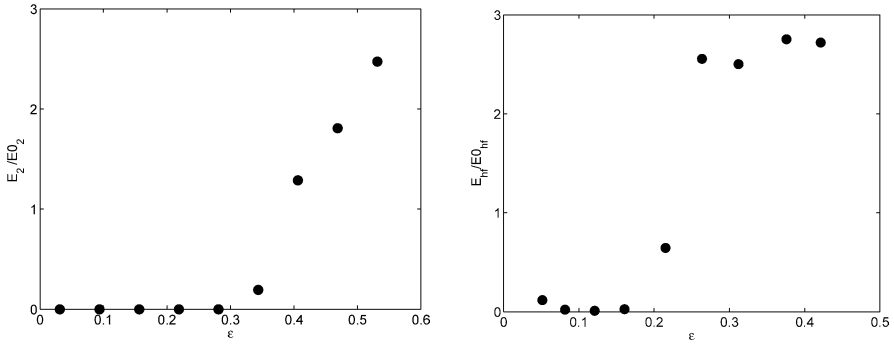

(a) (b)

Fig. 12. Energy ratio in the harmonic (a): modes of model equation system, and (b): frequencies of the experiments. E_{hf} and E_2 are the value with $G_{1,\mathrm{opt}}$, where $E0_{\mathrm{hf}}$ and $E0_2$ is the value without control.

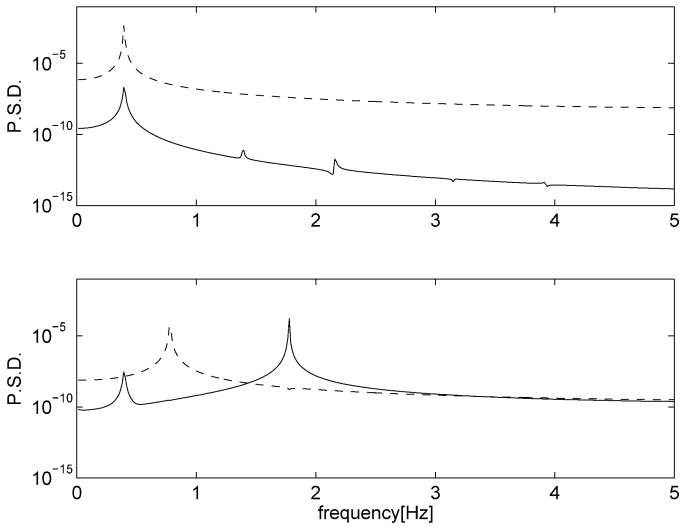

Fig. 13. Spectra of the fundamental (top) and harmonic (bottom) modes with (solid line) and without (dashed line) control.

solid/dashed lines. The spectra of asymmetric harmonic modes are omitted since they are the same as symmetric harmonic modes. With control, as the attenuation of the energy can be seen on the original fundamental and harmonic frequencies which respectively belong to fundamental and harmonic modes, there is another peak in the spectrum of the harmonic modes at the frequency of 1.78 Hz. Since this is not an overtone of any of the original temporal modes, it should be the result of linear destabilization of the harmonic modes.

5.5. *Optimal positioning of controllers*

For the above case ($x_1 = 0.25$ and $x_2 = 0.5$), controlability and observability matrix can be computed as, $\Gamma|_{\mathbf{B}=\mathbf{B_p}} = \Omega|_{\mathbf{C}=\mathbf{C_p}} = 12$. Hence the linear system is neither controllable nor observable. Note that, despite this fact, the control still works in the regime with $\epsilon \ll 1$. When the influence of the harmonic modes is small, it is more suitable to judge the controllability of the system by computing the criterion for a linear system with only fundamental modes. In this case, with the same local actuation, the resulting system was confirmed to be controllable. As ϵ increases, the energy in the harmonic modes grow with respect to the fundamental mode (Fig. 4) and the harmonic modes need to be taken into account. Therefore, the controllability should be determined based on the full linear system (43). Although, in this regime, the suppression to some extent can still be obtained, this is purely attributed to the attenuation of the fundamental modes. The loss of controlability of the full linear system is understandable from the physical picture. Since the original idea in the previous experiment was to target the fundamental mode, the heaters were positioned with a phase difference of $\pi/2$ to control both sine and cosine waves of the fundamental modes at the same time. However, for the harmonic modes, the phase difference is π, hence does not cover two

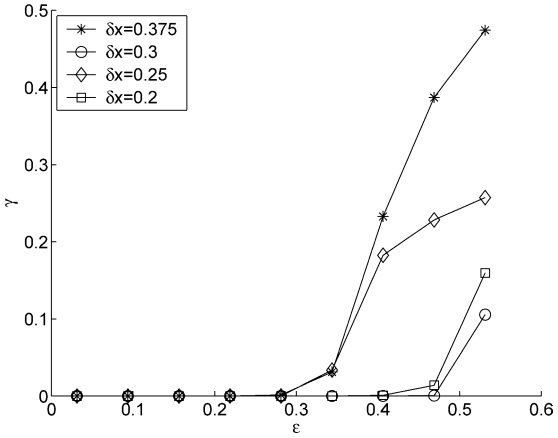

Fig. 14. Optimizing the configuration of the controllers. $G_1 = G_{1,\mathrm{opt}}$, $x_2 = 0.5$.

degrees of freedom, sine and cosine modes. Therefore the remedy would be to change the heater positions so that the phase differences for neither of the mode becomes a multiple of $\pi/2$. Doing so, we obtain $\Gamma = 18$ therefore the system is controllable. With the same argument, system becomes observable with the corresponding change in the sensor position.

In the current study, we limit the control scheme to be a simple one of the experiments where sensor signals are fedback to paired heaters with common constant control gain. With such a restriction, the satisfaction of the controllability merely suggest the possibility to act on all the existing linear modes and does not necessarily mean better control. The effectiveness of control should certainly depend also on the positions of the sensors and heaters. The dependence of the control performance on the positioning of the controllers was experimentally investigated by Shiomi and Amberg [14], however it was based on the measurements of a coarse variation of the parameters corresponding to $\delta x = |x_1 - x_2| = 0.25, 0.375$ in the current study. Using the toy model, the investigation can be carried out with finer parameter variation. Results obtained by applying the feedback control is shown in Fig. 14, where the overall performance of the control for various value of x_1 is plotted. The value of x_2 is fixed to 0.5. Ranging δx from 0.2 to 0.375, significant improvement of the performance was achieved with the best performance when $\delta x = 0.3$. With this positioning, the criticality is delayed to $\epsilon \sim 0.47$.

The result shows a certain agreement with the experiment where control performs better for $\delta x = 0.25$ than for $\delta x = 0.375$. The analysis also suggests that we may have jumped over the optimal positioning when varying δx in the experiment. Of course, there are some questions of the relevancy of the analysis. For instance, in the experiment, the cause which limits the performance of the control is not evident. Hence, when varying the positioning of sensors and heaters, it is not clear yet if the limitation is caused by the appearance of the same wavenumber mode. The selection of the destabilized mode can naturally be dependent on the configuration of the sensors and heaters. However, the fact that the amplification of the harmonic frequency components observed independently of δx gives rise to a speculation that the newly appearing mode might be always the harmonic one.

6. Conclusions

To fill the lack of understanding in how the proportional control method influences the system, a simple model problem was formulated. Limiting the number of azimuthal modes to the fundamental and first harmonic modes and roughly assuming the other spatial profiles, a set of ordinary differential equations was obtained. The model is formulated to show the basic features of the system such as standing/traveling wave structures and Hopf bifurcation. The model system has open parameters so that it could be calibrated to the given physical system. Implementing the feedback control to this toy model, we could capture some of the essential qualitative features of the influence of the control. As shown in Figs. 11 and 12, the suppression ratio increases rapidly over a certain threshold value of ϵ due to the destabilization of the harmonic modes.

In spite of the rough estimations made in the derivation of the model system, the model shows very good qualitative agreement with the experimental results, not only for the uncontrolled system but also for the controlled one. The result of this study suggests that the performance of the linear control with local temperature modification may be limited due to the linear destabilization of the harmonic modes.

There is a certain discrepancy in the behaviors of the controlled oscillation in current system and the experiments which one may need to consider before concluding that this study describes the definite cause of the limitation of the control performance. The linear harmonic mode has its own peak in almost double the overtone frequency of the fundamental mode, which does

not match the observation in the experiment. It is possible that, in the experiment, the linear harmonic modes and nonlinear harmonic modes have similar critical frequency, but it is far from certain. Nevertheless the present study points out the possibility of destabilizing the harmonic modes of the target modes due to the finite length of the actuator though, instinctively, this goes against the characteristic of this control method where any waves that are in phase at sensor/heater positions were thought to be suppressed to some extent.

It should be noted that due to the locality of the actuator and coupling of fundamental and harmonic modes, the linear controllability can be satisfied with fewer actuators than the ideal case. This confirms the practicability of suppression of the oscillation using the current proportional control method which was applied in the previous experiments without any theoretical assurance. Optimizing the positioning of the controller in connection with the linear controllability, the control performance could be improved to a significant extent. The result of the analysis agrees well with that found in experiments and suggests the possibility of improving the control performance in the experiments by adopting finer parameterization of the controller positions

In the case demonstrated in the current report, the solution was limited to have only a single fundamental mode for sake of simplicity. The number of modes can easily be increased by adding more terms in the solution in order to make the model system applicable to the cases where multiple linear modes appear as in Shiomi et al. [15]. In this case, however, the calibration process would be difficult since the model would need to be calibrated against the controlled system.

Acknowledgements

This work was supported by the Swedish Research Council (VR).

Appendix. Designing the gain matrix

A general expression of the wave of the ith mode traveling/standing in the x-direction is,

$$\theta_i'(x,t) = A_{i,+}(t)\sin(2i\pi x - 2\pi f_i t + \eta_{i,1}) + A_{i,-}(t)\sin(2i\pi x + 2\pi f_i t + \eta_{i,2}), \tag{56}$$

where $\eta_{i,1}$ and $\eta_{i,2}$ are the phases of the positive and negative propagating waves of mode (wavenumber in x-direction) i, respectively, and f_i denotes the critical frequency of the ith mode. The critical frequencies, f_n, were detected from the peaks of the power spectra. The temperature signals at the sensors, $\theta_i'(x_1,t)$, $\theta_i'(x_2,t)$, $\partial\theta_i'(x_1,t)/\partial t$ and $\partial\theta_i'(x_2,t)/\partial t$ can expressed as functions of $A_{i,+}(t)$, $A_{i,-}(t)$, $\eta_{i,1}$ and $\eta_{i,2}$. Hence, knowing the former 4 variables, the latter ones can be computed.

Now, we intend to compute the linear gain matrix $\mathbf{K}$ with which the best opposition against θ_1' can be obtained. Inputs are the two temperature signals of the fundamental oscillation at $x = x_1$ and x_2. For the sake of convenience in formulation, Eq. (56) is rewritten as

$$\theta_1'(x,t) = \sum_{j=1}^{4} A_j^*(t)\chi_j(\phi,t), \tag{57}$$

where $\chi = \{\sin[2\pi(x+f_1t)], \cos[2\pi(x+f_1t)], \sin[2\pi(x-f_1t)], \cos[2\pi(x-f_1t)]\}$. Assuming that the cancellation of the disturbance is done by adding the temperature proportional to the surface heat conduction $q^*(x,t) = q|_{h=1}$, the objective function can be written as,

$$J = \int_0^1 (\theta_1' - q^*)^2\,\mathrm{d}x, \tag{58}$$

which is a quadratic function of A_j^* and q_i. Now we calculate the optimal value with respect to the outputs q_i, $i = 1, 2$,

$$\frac{\partial J}{\partial q_i} = 0. \tag{59}$$

Solving the linear equations, q_i can be expressed as linear functions of A_j^*. Substituting, x_1, x_2, $\theta_1'(x_1,t)$, $\theta_1'(x_2,t)$, $\partial\theta_1'(x_1,t)/\partial t$ and $\partial\theta_1'(x_2,t)/\partial t$ into A_j^*, the expression is reduced to,

$$\begin{bmatrix} q_1(t) \\ q_2(t) \end{bmatrix} = \mathbf{K}\begin{bmatrix} \theta_1'(x_1,t) \\ \theta_1'(x_2,t) \end{bmatrix} \tag{60}$$

with constant elements in the 2×2 matrix, **K**. The time-dependent parts and the time derivatives spontaneously drop out from the expression. The values of **K** were computed for a range of x_1 and x_2 for the given size of the actuator. As a consequence, the optimal **K** was found to have diagonal elements several orders higher than the non-diagonal elements.

References

[1] C.E. Chang, W.R. Wilcox, Analysis of surface tension driven flow in floating zone melting, Int. J. Heat Mass Transfer 19 (1976) 355–356.
[2] D. Schwabe, A. Scharmann, Some evidence for the existence and magnitude of a critical Marangoni number for the onset of oscillatory flow in crystal growth melts, J. Cryst. Growth 6 (1979) 125–131.
[3] C.H. Chun, W. Wuest, Experiments on the transition from the steady to the oscillatory Marangoni-convection of a floating zone under reduced gravity effect, Acta Astron. 6 (1979) 1073–1082.
[4] M.K. Smith, S.H. Davis, Instability of dynamic thermocapillary liquid layers, J. Fluid Mech. 132 (1983) 119.
[5] M. Wanschura, V.M. Shevtsova, H.C. Kuhlmann, H.J. Rath, Convective instability mechanisms in thermocapillary liquid bridges, Phys. Fluids 7 (1995) 912–925.
[6] M. Levenstam, G. Amberg, Hydrodynamical instabilities of thermocapillary flow in a half-zone, J. Fluid Mech. 297 (1995) 357–372.
[7] F. Preisser, D. Schwabe, A. Scharmann, Steady and oscillatory thermocapillary convection in liquid columns with free cylindrical surface, J. Fluid Mech. 126 (1983) 545–567.
[8] J. Leypoldt, H.C. Kuhlmann, H.J. Rath, Three-dimensional numerical simulation of thermocapillary flows of cylindrical liquid bridges, J. Fluid Mech. 414 (2000) 285–314.
[9] I. Ueno, S. Tanaka, H. Kawamura, Oscillatory and chaotic thermocapillary convection in a half-zone liquid bridge, Phys. Fluids 15 (2003) 408–416.
[10] S. Benz, P. Hinz, R.J. Riley, G.P. Neitzel, Instability of thermocapillary–buoyancy convection in shallow layers. Part 2. Suppression of hydrothermal waves, J. Fluid Mech. 359 (1998) 165–180.
[11] V. Petrov, M.F. Schatz, K.A. Muehlner, S.J. VanHook, W.D. McCormick, J.B. Swift, H.L. Swinney, Nonlinear control of remote unstable states in a liquid bridge convection experiment, Phys. Rev. Lett. 77 (1996) 3779–3782.
[12] V. Petrov, K.A. Muehlner, S.J. VanHook, H.L. Swinney, Model-independent nonlinear control algorithm with application to a liquid bridge experiment, Phys. Rev. E 58 (1998) 427–433.
[13] J. Shiomi, G. Amberg, P.H. Alfredsson, Active control of oscillatory thermocapillary convection, Phys. Rev. E 64 (2001) 031205.
[14] J. Shiomi, G. Amberg, Active control of a global thermocapillary instability, Phys. Fluids 14 (2002) 3039–3045.
[15] J. Shiomi, M. Kudo, I. Ueno, H. Kawamura, G. Amberg, Feedback control of oscillatory thermocapillary convection in a half-zone liquid bridge, J. Fluid Mech. 496 (2003) 193–211.
[16] H.H. Bau, K.E. Torrance, Transient and steady bahavior of an open, symmetrically-heated, free convection loop, Int. J. Heat Mass Transfer 24 (1981) 597–609.
[17] D. Canright, Thermocapillary flow near a cold wall, Phys. Fluids 6 (1994) 1415–1424.
[18] R. Savino, R. Monti, Oscillatory Marangoni convection in cylindrical liquid bridges, Phys. Fluids 8 (1996) 2906–2922.
[19] R. Monti, R. Fortezza, D. Castenuto, G. Desiders, The telemaxus experiment on oscillatory Marangoni flow, ESA SP 1132 (4) (1994) 44.
[20] Y. Kamotani, S. Ostrach, J. Masud, Microgravity experiment and analysis of oscillatory thermocapillary flows in cylindrical container, J. Fluid Mech. 410 (2000) 211–233.
[21] B.-C. Sim, A. Zebib, Effect of free surface heat loss and rotation on transition to oscillatory thermocapillary convection, Phys. Fluids 14 (2002) 225–231.
[22] R. Lavalley, G. Amberg, H. Alfredsson, Experimental and numerical investigation of nonlinear thermocapillary oscillations in an annular geometry, Eur. J. Mech. B Fluids 20 (2001) 771–797.
[23] Y. Kamotani, J.H. Lee, S. Ostrach, A. Pline, An experimental study of oscillatory thermocapillary convection in cylindrical containers, Phys. Fluids A 4 (1991) 955–962.
[24] T. Kailath, Linear Systems, first ed., Prentice-Hall, 1980.